Journal of Genetics and Genomics 46 (2019) 259–267

Contents lists available at ScienceDirect

Journal of Genetics and Genomics

Journal homepage: www.journals.elsevier.com/journal-of-genetics-and-genomics/

Original research

Arabidopsis AGC protein kinases IREH1 and IRE3 control root skewing

Xiaozhen Yue [a, b], Zhiai Guo [a], Teng Shi [a, b], Lizhen Song [a], Youfa Cheng [a, b, *]

[a] Key Laboratory of Plant Molecular Physiology, Institute of Botany, Chinese Academy of Sciences, Beijing 100093, China
[b] University of Chinese Academy of Sciences, Beijing 100049, China

ARTICLE INFO

Article history:
Received 26 November 2018
Received in revised form
4 February 2019
Accepted 25 February 2019
Available online 22 March 2019

Keywords:
AGC kinases
IREH1
IRE3
Root skewing
Microtubule
Arabidopsis

ABSTRACT

AGC protein kinases play important roles in plant growth and development. Several AGC kinases in *Arabidopsis* have been functionally characterized. However, the "AGC Other" subfamily, including IRE, IREH1, IRE3 and IRE4, has not been well understood. Here, we reported that *ireh1* mutants displayed a root skewing phenotype, which can be enhanced by *ire3* mutation. *IREH1* and *IRE3* were expressed in roots, consistent with their function in controlling root skewing. The fluorescence intensities of the microtubule marker *KNpro*:EGFP-MBD were decreased in *ireh1*, *ire3* and *ireh1 ire3* mutants compared to wild type. The microtubule arrangements in *ireh1* and *ireh1 ire3* mutants were also altered. IREH1 physically interacted with IRE3 *in vitro* and *in planta*. Thus, our findings demonstrate that IREH1 and IRE3 protein kinases play important roles in controlling root skewing, and maintaining microtubule network in *Arabidopsis*.

Copyright © 2019, Institute of Genetics and Developmental Biology, Chinese Academy of Sciences, and Genetics Society of China. Published by Elsevier Limited and Science Press. All rights reserved.

1. Introduction

AGC kinases (cAMP-dependent protein kinase A, cGMP-dependent protein kinase G and phospholipid-dependent protein kinase C) play crucial roles in regulating plant growth and development (Bögre, 2003; Pearce et al., 2010). The 39 AGC kinases in *Arabidopsis* can be divided into six subfamilies: AGC VIIIa, AGC VIIIb, AGC VII, AGC VI, AGC Other, and PDK1 subfamilies, according to the protein kinase classification based on the catalytic domain (Bögre, 2003). Members of the AGC VIIIa subfamily have been shown to control multiple development processes by modulating auxin actions, such as PID/PID2/WAG1/WAG2, D6PK/D6PKLs, AGC1-12, and PAX/PAXL (Christensen et al., 2000; Cheng et al., 2008; Zourelidou et al., 2009; Willige et al., 2013; Haga et al., 2018; Marhava et al., 2018). In the AGC VIIIb subfamily, UCN and UCNL redundantly regulate planar growth of integuments, and PHOT1/2, two blue light receptors, control phototropism and chloroplast relocation (Briggs and Christie, 2002; Enugutti et al., 2012). The AGC Other subfamily has four members: IRE, IREH1, IRE3 and IRE4. It has been reported that IRE plays a role in root hair growth (Oyama et al., 2002), but the role of rest members in *Arabidopsis* development has not been well understood.

Roots are very important especially in anchoring plants and absorbing nutrition and water from the soil. During plant growth, roots respond to multiple environmental stimuli, such as gravity, light, touch, moisture and nutrition. These environmental cues and intrinsic factors regulate root growth pattern and maintain normal direction of cell expansion (Roy and Bassham, 2014). Several mutants of microtubule proteins and microtubule-associated proteins showed root skewing or waving phenotypes, such as the left-handed mutants *lefty1*, *lefty2*, and *eb1b* (Whittington et al., 2001; Thitamadee et al., 2002; Bisgrove et al., 2008), and the right-handed mutants *spr1* and *spr2* (Nakajima et al., 2004; Shoji et al., 2004). In the mutants of WVD2 (a microtubule-associated protein) and TNO1 (a TGN-localized SNARE-interacting protein), changes of microtubule orientation and dynamics caused root skewing (Perrin et al., 2007; Roy and Bassham, 2017).

In order to understand the role of *IREH1* and *IRE3* of AGC Other subfamily in *Arabidopsis* growth and development, we isolated and characterized their loss-of-function mutants. We found that *ireh1* mutants displayed a root skewing phenotype, which can be enhanced by *ire3*. The arrangements of microtubules and the responses to the microtubule drug in the *ireh1* and *ireh1 ire3* mutants were also altered. IREH1 interacted with IRE3 *in vitro* and *in planta*. These findings demonstrate that AGC protein kinases IREH1 and IRE3 control root skewing and maintain microtubule network in *Arabidopsis*.

* Corresponding author.
E-mail address: yfcheng@ibcas.ac.cn (Y. Cheng).

https://doi.org/10.1016/j.jgg.2019.02.007
1673-8527/Copyright © 2019, Institute of Genetics and Developmental Biology, Chinese Academy of Sciences, and Genetics Society of China. Published by Elsevier Limited and Science Press. All rights reserved.

2. Results

2.1. Isolation and characterization of ireh1 and ire3 mutants

To investigate the role of *IREH1* in *Arabidopsis* growth and development, we obtained two T-DNA insertion lines *ireh1-1* and *ireh1-2* (in Col-0 background) from the *Arabidopsis* Stock Center (Fig. 1A). RT-PCR analysis confirmed that the expression of *IREH1* in both mutant alleles was knocked out (Fig. 1B), indicating that they were null alleles. When grown vertically on MS plates and observed from the top, the roots of both *ireh1* alleles skewed to the left of the gravity, while the primary roots of wild-type (WT) seedlings were basically along with the gravity vector (Fig. 1C–E). A closer look of the *ireh1* roots revealed that the epidermal cell files rotated to the right (Fig. 1F and G). Because *IRE3* is the closest homolog of *IREH1* (Fig. S1), we asked if they have redundant functions. Two T-DNA lines *ire3-1* (in Col-0 background) and *ire3-2* (in Ws background) were characterized (Fig. 1A and B). The *ire3* single mutants exhibited similar root skewing angles and epidermal cell file rotation angles to their WT seedlings, but the *ireh1 ire3* double mutants displayed much bigger root skewing angles and cell file rotation angles than the *ireh1* single mutants (Figs. 1D, 1E and S2), indicating that *IREH1* and *IRE3* had an overlapping function in controlling the root epidermal cell file rotation. Since all combinations of *ireh1 ire3* double mutants displayed similar phenotypes, and both *ireh1-1* and *ire3-1* were in Col-0 background, we used them in the next experiments.

2.2. Expression patterns of IREH1 and IRE3

To reveal the expression patterns of *IREH1* and *IRE3*, we generated the *IREH1-GUS* and *IRE3-GUS* transgenic lines, each of which harbored a genomic DNA fragment containing the coding and

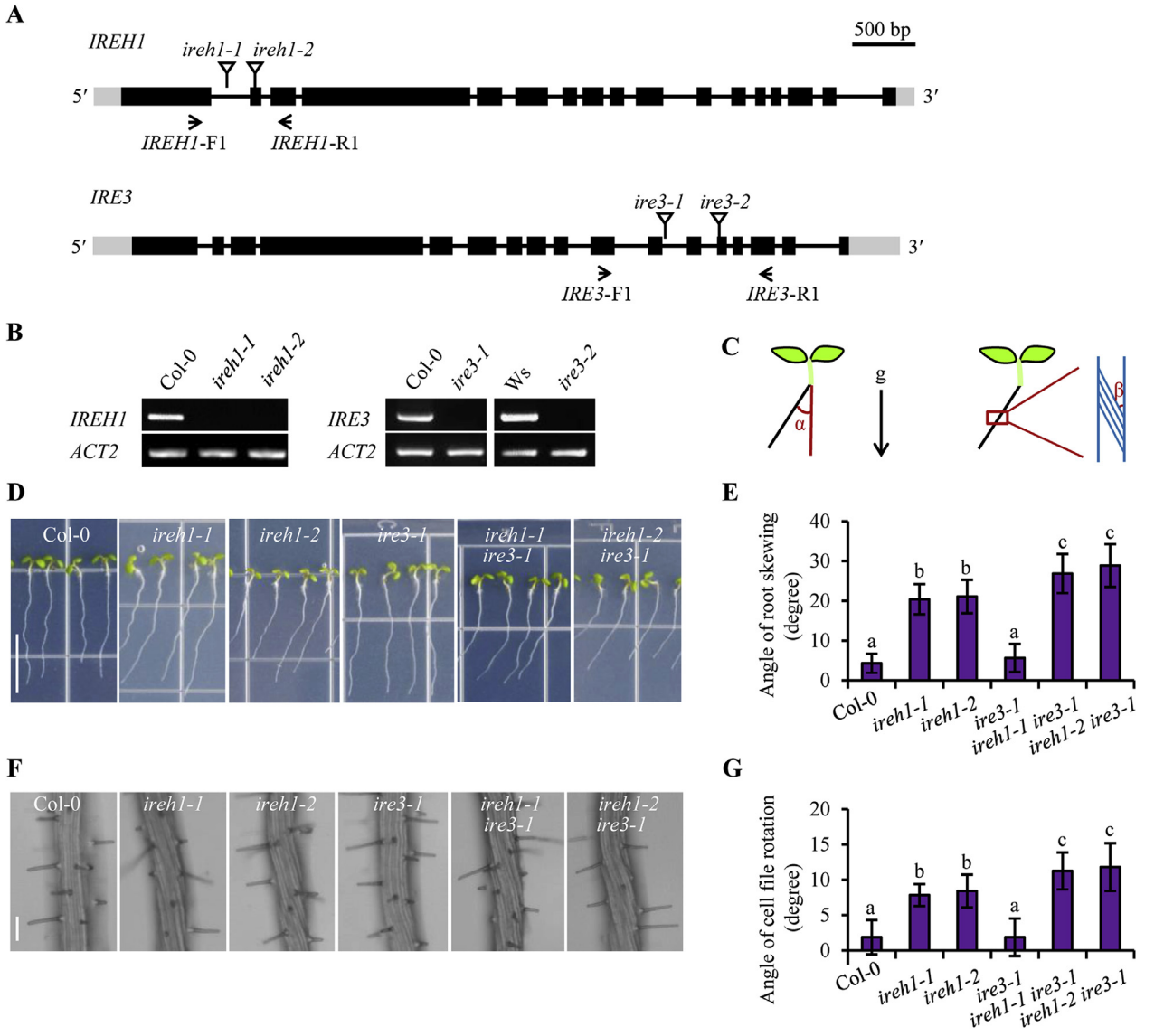

Fig. 1. *ireh1* and *ireh1 ire3* mutants display root skewing phenotypes. **A**: Schematic structure of *IREH1* and *IRE3* genes. Black boxes, lines and grey boxes refer to exons, introns and 5′UTR/3′UTR, respectively. T-DNA insertion sites and primer locations are shown as triangles and arrows, respectively. **B**: Expression analysis of *IREH1* and *IRE3* in 8-day-old wild-type (Col-0 or Ws) and mutant seedlings by RT-PCR. *ACT2* served as a control. **C**: Schematic illustration of root skewing angle (α) and epidermal cell file rotation angle (β). g, gravity. **D**: 6-day-old seedlings grown on vertical plates. Note root skewing in *ireh1* and *ireh1 ire3* mutants. **E**: Quantification of the root skewing angles. **F**: Right-handed epidermal cell file rotation in the root maturation zone of *ireh1* and *ireh1 ire3* mutants. **G**: Quantification of cell file rotation angles. Statistical analysis was performed using a one-way ANOVA followed by LSD test. Values are means ± SE ($n = 25$). Different letters represent significant differences at $P < 0.01$. Pictures in **D** and **F** were taken from the surface of the medium. Scale bars: 1 cm (**D**) and 100 μm (**F**).

regulatory sequences of *IREH1* or *IRE3* immediately followed by the *GUS* gene before the stop codon. Over 20 individual 5-day-old T_2 transgenic seedlings were analyzed. As shown in Fig. 2, at the seedling stage, both *IREH1-GUS* and *IRE3-GUS* signals were detected in cotyledons (Fig. 2A and J), new true leaves (Fig. 2B and K), primary and lateral roots (Fig. 2C–I and L–R). Notably, in the roots, *IREH1-GUS* and *IRE3-GUS* were expressed in the vascular tissues, root hairs, lateral root primordia and epidermis (Fig. 2C–I and L–R), consistent with their functions in controlling root cell file rotation.

2.3. The orientation of cortical microtubules was altered in epidermal cells of ireh1 and ireh1 ire3 roots

The orientation of cortical microtubules is generally believed to specify the orientation of nascent cellulose microfibrils, thereby dictating the direction of cell elongation. Several root skewing mutants showed diverse arrangements of cortical microtubules in root epidermal cells of elongation zone, and most of them were sensitive to microtubule drugs, suggesting that most of these genes were related to microtubule function (Furutani et al., 2000; Thitamadee et al., 2002). To explore if the root skewing phenotypes of *ireh1* and *ireh1 ire3* mutants were caused by alteration of cortical microtubule arrangement, we introduced the microtubule marker *KNpro*:EGFP-MBD (Wang and Huang, 2014) into *ireh1-1*, *ire3-1*, and *ireh1-1 ire3-1*, respectively, by crossing.

In the meristem and elongation zones, the cortical microtubule arrays of epidermal cells in *ireh1-1*, *ire3-1* and *ireh1-1 ire3-1* mutants were similar to those of WT. The directions of microtubules were almost perpendicular to the direction of root growth and parallel to each other (Fig. 3A and B). In the maturation zone, the microtubule arrays of epidermal cells in WT and *ire3-1* aligned obliquely and largely toward one direction, with less than 5% in different directions; however, in *ireh1-1* and *ireh1-1 ire3-1* mutants, over 30% of the microtubule arrays were arranged in different directions (Fig. 3C, G and H). The fluorescence intensities of microtubule network in meristem, elongation and maturation zones were all significantly decreased in *ireh1-1*, *ire3-1* and *ireh1-1 ire3-1* mutants compared to WT, but no significant difference was found between the mutants (Fig. 3D–F). Because the fluorescence intensity reflects the stability and density of microtubules, our observations on microtubule arrangement and intensity indicate that both *IREH1* and *IRE3* are important for maintaining the microtubule network. Interestingly, the *ire3* mutant also exhibited the decreased fluorescence intensities of microtubules; however, it did not display root skewing, suggesting that the root skewing is unlikely due to the decreased microtubule intensity.

2.4. ireh1 and ireh1 ire3 were less sensitive to the microtubule drug treatment

Oryzalin is thought to bind with tubulin and promote depolymerization of microtubules (Morejohn, 1991). When applied to intact plants at concentrations above certain thresholds, it severely inhibits shoot and root growth, and causes extensive radial swelling in some types of treated cells (Morejohn, 1991; Baskin et al., 1994; Hasenstein et al., 1999). To further confirm the association of *IREH1* and *IRE3* with microtubules, we examined the root growth response upon oryzalin treatment. When grown on the plate with 0.1 μM or 0.2 μM oryzalin, the inhibition of primary root elongation in *ireh1-1* and *ireh1-1 ire3-1* mutants was less than WT and *ire3-1* (Fig. 4A and B). In terms of the root cell swelling, when grown on the plates with 0.2 μM and 0.3 μM oryzalin, *ireh1-1* and *ireh1-1 ire3-1* mutants were

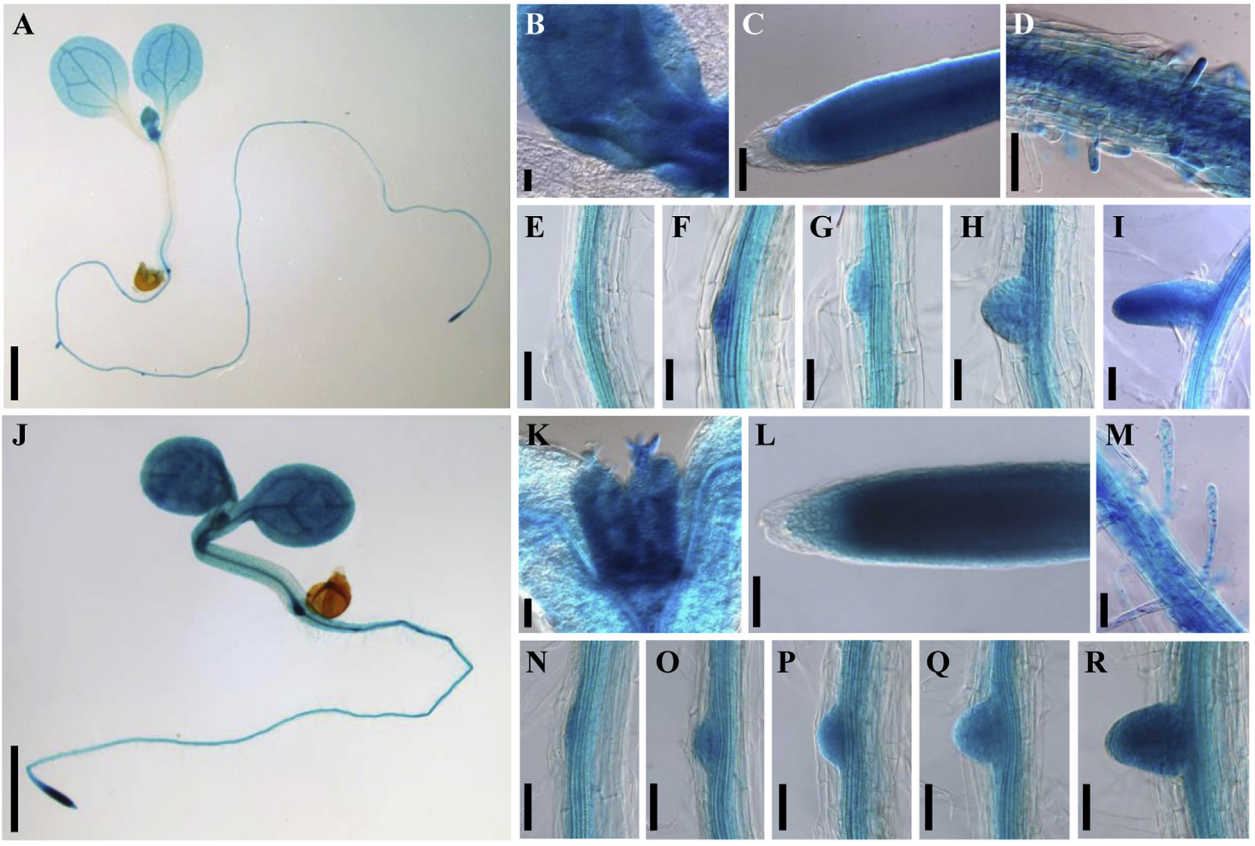

Fig. 2. Expression patterns of *IREH1* and *IRE3*. Expression of *IREH1-GUS* (**A**–**I**) and *IRE3-GUS* (**J**–**R**) in 5-day-old seedlings: cotyledons (**A** and **J**), true leaves (**B** and **K**), root tip (**C** and **L**), root hairs (**D** and **M**), lateral roots (**E**–**I** and **N**–**R**). Scale bars: 1 mm (**A** and **J**) and 50 μm (**B**–**I** and **K**–**R**).

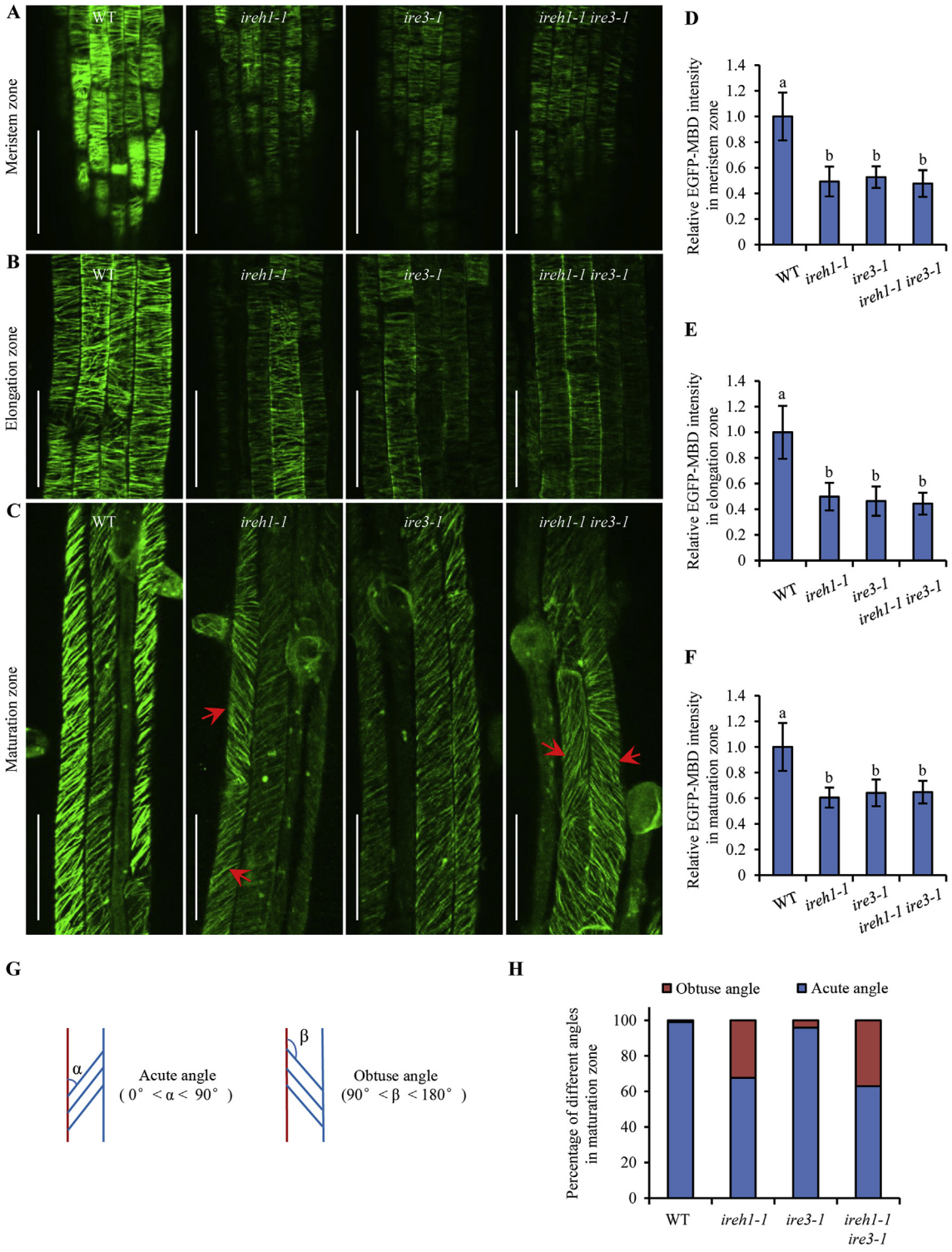

Fig. 3. Cortical microtubule arrays in root epidermal cells. **A**–**C**: Fluorescence analysis of the cortical microtubule arrangement and intensity of root epidermal cells of 5-day-old seedlings in the meristem zone (**A**), elongation zone (**B**) and maturation zone (**C**). Microtubule arrangements were largely perpendicular to the direction of cell elongation in WT and mutants in the meristem and elongation zones. In the maturation zone, microtubule arrangements were nearly in similar directions in WT and *ire3-1*, but often in different directions in different cells (red arrows) in *ireh1-1* and *ire1-1 ire3-1* mutants. $n = 20$ seedlings per genotype. Scale bars: 50 μm. **D**–**F**: Quantification of the relative fluorescence intensities of EGFP-MBD in the meristem zone (**D**), elongation zone (**E**) and maturation zone (**F**). The fluorescence intensities in WT were set as an arbitrary unit 1. Statistical analysis was performed using a one-way ANOVA followed by LSD test. Values are means ± SE of 45 cells per genotype in total (15 roots and 3 cells per root). Different letters represent significant differences at $P < 0.01$. **G**: Schematic illustration of the angles between the left side of the cell and microtubule arrays, acute angle (α) and obtuse angle (β). **H**: Percentage of microtubule arrangement angles in the maturation zone. 75 cells (25 roots and 3 cells per root) were measured per genotype.

less sensitive than WT and *ire3-1* (Fig. 4C). These results further demonstrated that IREH1 and IRE3 are related to microtubule function, although the underlying mechanism is still unclear.

2.5. IREH1 physically interacted with IRE3

The genetic interaction between *IREH1* and *IRE3* implied that they may function together to regulate *Arabidopsis* root skewing. To gain insights of the underlying mechanisms, we carried out the immunoprecipitation-mass spectrometry (IP-MS) experiments to identify the proteins interacting with IREH1. We first generated *Arabidopsis* transgenic plants by transforming *pPZP211-IREH1gDNA-GFP* into *ireh1-1* mutant. The transgene was able to rescue the root skewing phenotype of *ireh1-1* mutant, indicating that the IREH1-GFP was functional. The IP-MS experiments were then performed using the T_2 plants with the *IREH1-GFP* transgene and identified a peptide fragment of IRE3 (IQEKYLQLCELMDDEKGTIIDEDAPLEDDVVR), suggesting IRE3 is an IREH1-interacting protein. To validate the physical interaction between IREH1 and IRE3, we carried out yeast two-hybrid, Co-IP and luciferase complementation imaging (LCI) assays (Fig. 5).

In the yeast two-hybrid assay, yeast cells co-transformed with vectors encoding IREH1 fused with AD domain (IREH1-AD) and IRE3 fused with BD domain (IRE3-BD) were able to grow and display blue color on the SD quadruple dropout medium supplemented with X-α-Gal (Fig. 5A). Similar result was obtained when the yeast cells were co-transformed with vectors encoding IREH1-BD and IRE3-AD (Fig. 5A). However, the negative controls were not able to survive (Fig. 5A). These results indicated that IRE3 can interact with IREH1 in yeast cells.

We further verified the IREH1-IRE3 interaction by the Co-IP assay. Two constructs *pSuper1300-IREH1-Flag* and *pSuper1300-IRE3-GFP* were co-transformed into *Nicotiana benthamiana* leaves via *Agrobacterium*-mediated transformation. Three days after transformation, total proteins were extracted from leaves and Co-IP was performed using the anti-GFPmAb-agarose. The proteins associated to the anti-GFPmAb-agarose were separated on the SDS-PAGE gel and then transferred to a PVDF membrane. The IRE3-GFP protein was detected with GFP antibody, and IREH1-Flag was detected by the Flag antibody (Fig. 5B), indicating that IRE3 interacted with IREH1 in the Co-IP assay.

Moreover, we carried out the LCI assay in tobacco leaves. Two constructs *pCAMBIA1300-IREH1-nLUC* and *pCAMBIA1300-cLUC-IRE3* were co-transformed into *N. benthamiana* leaves via *Agrobacterium*-mediated transformation, and the luciferase activity signal was detected in the leaf area three days after transformation; however, no signals were detected in the leaf areas transformed with other combinations (Fig. 5C). Thus, the yeast two hybrid, Co-IP and LCI assays indicated that IREH1 physically interacts with IRE3 to control root skewing. IREH1 and IRE3 likely have partially overlapping function in root skewing, and IREH1 plays the dominant role.

3. Discussion

It has been shown that AGC kinases play crucial roles in many development processes, such as flower, embryo and root development (Barbosa et al., 2018). However, little is known about the function of the AGC Other subfamily. It has been reported that *Arabidopsis IRE* plays a role in root hair elongation (Oyama et al., 2002). In this study, we demonstrated that *IREH1* and *IRE3* control root skewing and cell file rotation in *Arabidopsis*. Several root skewing mutants have been reported in *Arabidopsis*, which are caused by mutations in α-tubulins 6 and 4 (*lefty1* and *lefty2*) (Thitamadee et al., 2002), microtubule-interacting proteins (*spr1* and *spr2*) (Furutani et al., 2000), a protein similar to MAPK phosphatase (*phs1-1*) (Naoi and Hashimoto, 2004), a microtubule plus-end tracking protein (*eb1b*) (Bisgrove et al., 2008), and a KNAT1 transcription factor (*bp-1*) (Qi and Zheng, 2013). To our knowledge, IREH1 and IRE3 are the first AGC kinases found to control root skewing and cell file rotation in *Arabidopsis*.

The root skewing mutants often display epidermal cell file rotation, the degree of which correlates with the level of skewing. The handedness of the cell file rotation also correlates with the direction of skewing: left-handed cell file rotation for rightward skewing and right-handed cell file rotation for leftward skewing (Vaughn and Masson, 2011). This is also true in the *ireh1* and *ireh1 ire3* mutants. When observed from the top of the plate, the roots of *ireh1* and *ireh1 ire3* mutants skewed to the left of the gravity, while the epidermal cell files in the mutant roots rotated to the right. The degree of cell file rotation was correlated with the level of skewing, since *ireh1 ire3* displayed larger degrees of root skewing and cell file rotation than those of *ireh1* (Fig. 1D–G).

The cortical microtubules in root meristem and elongation zones of WT plants are arranged mostly in a transverse orientation, and mostly in an oblique orientation in root maturation zone (Vaughn and Masson, 2011). Although many skewing mutants have abnormal cortical microtubule arrays, some mutants did not display altered cortical microtubule arrays, including *spr2*, *eb1*, *spr1* and *tno1* (Furutani et al., 2000; Sedbrook et al., 2004; Bisgrove et al., 2008; Roy and Bassham, 2017). In the *ireh1* and *ireh1 ire3* mutants, we found that the cortical microtubule array orientation was abnormal in the maturation zone but was normal in the meristem and elongation zones (Fig. 3A–C). Because the cells in maturation zone already stop growth, it is unlikely that the abnormal orientation of microtubules in this zone directly caused the root skewing. In the root skewing mutant *tno1*, microtubule array orientation was unaffected in the root meristem, elongation and maturation zones; however, the maturation zone of mutant roots treated with the microtubule destabilization drug propyzamide (PPD) displayed malformed cells. It was proposed that the defects in the maturation zone of the PPD-treated *tno1* roots could then affect how the growing root interacts with the substrate, which would in turn affect root skewing (Roy and Bassham, 2017). Similarly, it is possible that in the root maturation zone of *ireh1* and *ireh1 ire3* mutants, the alterations in the epidermal cell file rotation and microtubule array orientation could affect the interaction between growing roots and the substrate, which would finally affect root skewing in an unknown mechanism.

IREH1 has been shown to be a protein kinase, at least with autophosphorylation activity, and the phosphorylation site was determined by mass spectrometry (de la Fuente van Bentem et al., 2008; Nemoto et al., 2011). IREH1 has been identified as one of the closest homologs of animal MASTs (microtubule-associated serine/threonine-protein kinases) with sequence and structural similarity (Karpov et al., 2010; Chudinova et al., 2017). In animals, MAST kinases are involved in regulation of microtubule protein phosphorylation (Valiente et al., 2005; Hain et al., 2014). Interestingly, MAST kinases form a highly conserved subfamily of AGC kinases (Pearce et al., 2010). We found that the microtubule arrangements were altered in the epidermal cells of maturation zone in *ireh1* and *ireh1 ire3* mutants. Moreover, the fluorescence intensities of the microtubule marker were significantly decreased in *ireh1*, *ire3* and *ireh1 ire3* mutants compared to wild type. These results suggested that IREH1 and IRE3 together control root skewing and cell file rotation, and maintain the cortical microtubule network. IREH1 and IRE3 likely have partially overlapping function in root skewing, and IREH1 plays the dominant role. It is also possible that both IREH1 and IRE3 are involved in the phosphorylation of unknown substrate proteins, and control root skewing and cortical microtubule network in an unknown manner. It would be interesting to explore the underlying mechanism in the future.

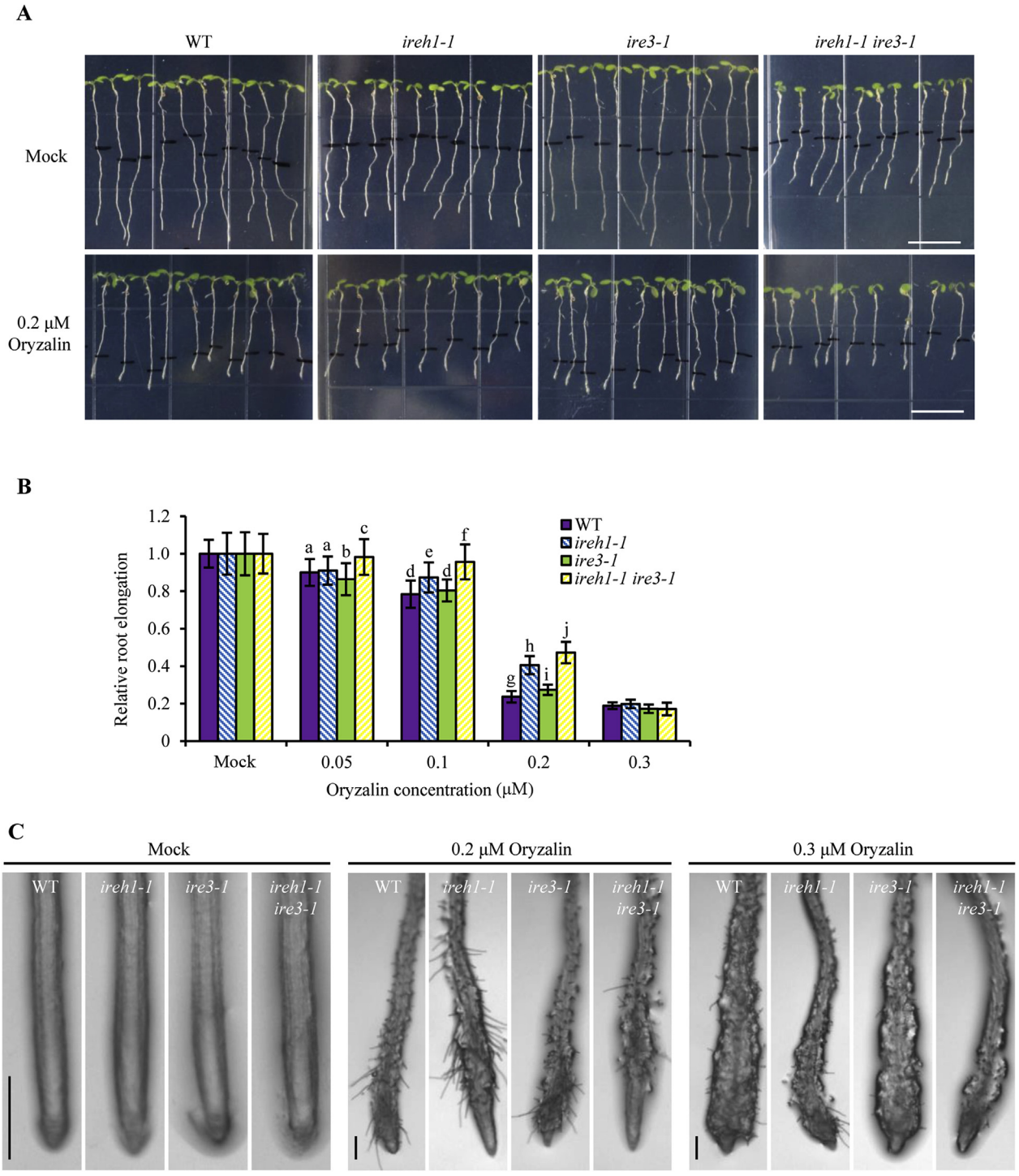

Fig. 4. *ireh1* and *ireh1 ire3* were less sensitive to the microtubule drug oryzalin. **A** and **B**: Representative images (**A**) and quantification (**B**) of the relative root elongation assay. The relative root elongation of *ireh1-1* and *ireh1-1 ire3-1* mutants were less inhibited than WT and *ire3-1* in the presence of 0.1 μM or 0.2 μM oryzalin. Seeds were sowed on 1/2 MS plates and placed vertically. Five-day-old seedlings were transferred onto 1/2 MS plates containing different concentrations of oryzalin to grow for 3 days. The positions of root tips were marked after transferring. Primary root length of untreated (mock) seedlings were set as an arbitrary unit 1. **C**: Root morphology of WT, *ireh1-1*, *ire3-1* and *ireh1-1 ire3-1* treated with 0.2 μM and 0.3 μM oryzalin. Statistical analysis was performed using a one-way ANOVA followed by LSD test. Values are means ± SE ($n = 25$). Different letters represent significant differences at $P < 0.05$. Treatments were repeated three times. Scale bars: 1 cm (**A**) and 200 μm (**C**).

4. Materials and methods

4.1. Plant materials and growth conditions

The T-DNA insertion mutants of *ireh1-1* (SALK_017861), *ireh1-2* (SALK_069962C), *ire3-1* (SALK_123447C), and *ire3-2* (FLAG_119B07) were obtained from *Arabidopsis* Stock Center. The T-DNA insertion sites were confirmed by sequencing of the PCR products of *ireh1-1* (869 bp after ATG), *ireh1-2* (1091 bp after ATG), *ire3-1* (4475 bp after ATG), and *ire3-2* (5145 bp after ATG). *ireh1-1*, *ireh1-2* and *ire3-1* were

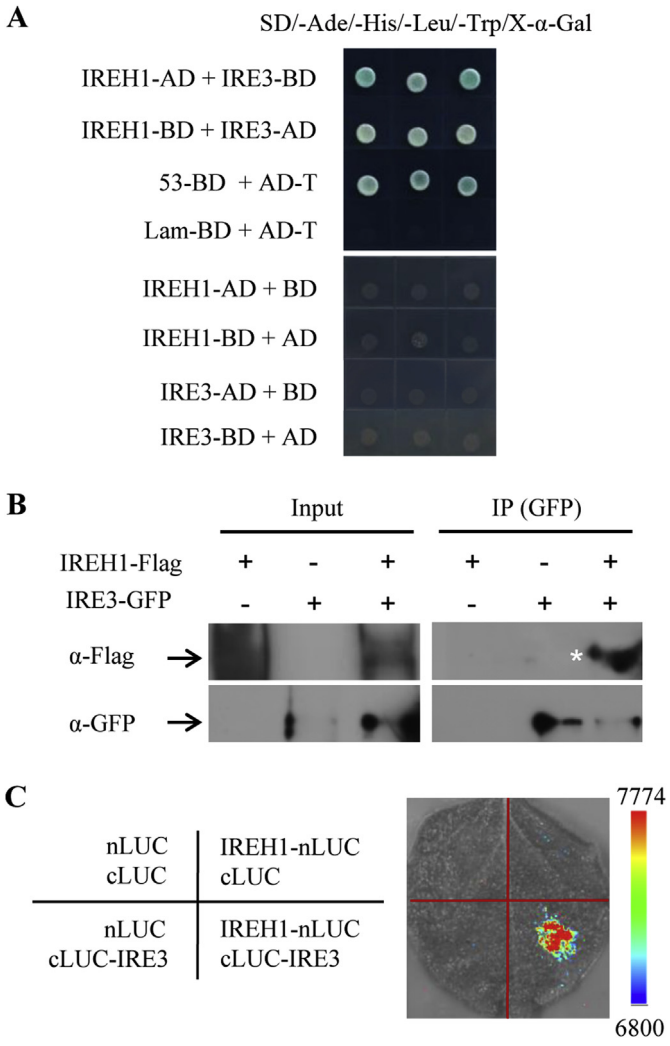

Fig. 5. IREH1 physically interacts with IRE3. **A**: Yeast two-hybrid assay. The 53-BD + AD-T and Lam-BD + AD-T were used as positive and negative controls, respectively. **B**: Co-IP assay in *N. benthamiana*. "GFP" in parenthesis denotes the anti-GFPmAb-agarose used in immunoprecipitation of each sample. Antibodies for immunoblotting are labeled at the left. The target interaction protein is marked with an asterisk. **C**: LCI assay in *N. benthamiana* leaf cells. Empty vectors were used as negative controls.

in the Col-0 background, and *ire3-2* was in the Ws background. *ireh1 ire3* double mutants were generated by crossing. All T-DNA insertion lines were genotyped as described previously (Cui et al., 2016). The genotyping primers are listed in Table S1. Seeds were sterilized and sowed on 1/2 Murashige and Skoog (MS) plates supplemented with 1.5% (w/v) sucrose and 0.8% (w/v) agar. The plates were kept in 4 °C for 3 days in dark before germination. Plants were grown under 16 h light/8 h dark at 22 °C.

For the oryzalin treatment, 5-day-old seedlings from vertical plates with 1/2 MS were transferred onto 1/2 MS plates containing different concentrations of oryzalin, and grew vertically for 3 days.

4.2. RNA extraction and reverse transcription

Total RNA of 8-day-old seedlings were isolated using EZgene™ Biozol RNA Kit (Biomiga, USA). Reverse transcription was performed using TransScript® First-Stand cDNA Synthesis Super Mix (Transgen, China). The RT-PCR primers are listed in Table S2.

4.3. Quantification of root lengths, root-skewing angles and cell file rotation angles

For relative root elongation measurement, seeds were sowed on 1/2 MS plates and placed vertically. Five-day-old seedlings were transferred onto 1/2 MS plates containing different concentrations of oryzalin to grow for 3 days. Root lengths and root widths were measured using NIH ImageJ software.

For the measurements of root-skewing angles and cell file rotation angles, seeds were sowed on 1/2 MS plates. Seedlings grew vertically for 6 days. The angles of root skewing and cell file rotation were analyzed by using NIH ImageJ software.

4.4. Plasmid construction and transgenic plants

To generate the *pPZP211-IREH1gDNA-GUS* and *pPZP211-IREH1gDNA-GFP* constructs, the genomic DNA fragment containing the 6392-bp coding region and 3788-bp upstream regulatory sequence of *IREH1* and the genomic DNA fragment containing the 609-bp downstream regulatory sequence of *IREH1* were amplified, respectively, by using two gene-specific primer pairs: ireh1gDNA-B-FP and ireh1gDNA-3P2-*Xba*I, and ireh1gDNA-5P1-*Xma*I and ireh1gDNA-A-RP. The amplified *IREH1* genomic DNA fragments were ligated into the *pPZP211* vector (Hajdukiewicz et al., 1994) at *Xma*I and *Xba*I sites using Gibson assembly method (Gibson et al., 2009) to produce the *pPZP211-IREH1gDNA* construct, which was then designed to introduce an *Afe*I site immediately before the stop codon. The resulting construct was digested with *Afe*I, and then the *GUS* gene or the *GFP* gene was inserted in frame to produce the *pPZP211-IREH1gDNA-GUS* or *pPZP211-IREH1gDNA-GFP* construct. The *GUS* gene was amplified by primers *Afe*I-GUS-5P and *Afe*I-GUS-3P(wsc). The *GFP* gene was amplified by primers *Afe*I-GFP-5P and *Afe*I-GFP-3P(wsc).

To generate *pPZP211-IRE3gDNA-GUS* construct, three genomic DNA fragments of *IRE3* including a 3098-bp upstream sequence, a 6253-bp coding region, and a 1659-bp downstream sequence were amplified by the gene-specific primer pairs: ire3gDNA-5P-*Xma*I and ire3gDNA-RP1, ire3gDNA-FP1 and ire3gDNA-RP2, ire3gDNA-FP2 and ire3gDNA-RP-*Apa*I, and ire3gDNA-FP-*Apa*I and ire3gDNA-3P-*Sal*I. The DNA fragments were ligated into the *pPZP211* vector at *Xma*I and *Sal*I sites to produce the *pPZP211-IRE3gDNA* construct, which was then designed to introduce an *Apa*I site immediately before the stop codon. The resulting construct was digested with *Apa*I, and then the *GUS* gene was inserted in frame to produce the *pPZP211-IRE3gDNA-GUS* construct. The *GUS* gene was amplified by primers *Apa*I-GUS-5P and *Apa*I-GUS-3P(wsc).

The *pPZP211-IREH1gDNA-GUS*, *pPZP211-IRE3gDNA-GUS* and *pPZP211-IREH1gDNA-GFP* constructs were transformed into *Agrobacterium tumefaciens* strain GV3101, and then transformed into *Arabidopsis* by floral dipping method (Clouth and Bent, 1998).

For the yeast two-hybrid assay, the full-length CDS of *IREH1* was amplified by primers ire-h1CDS(A)5P-*Bam*HI and ire-h1CDS(B)3P-*Pst*I, and cloned into *pGBKT7* with *Bam*HI and *Pst*I to generate *pGBKT7-IREH1*. The full-length CDS of *IREH1* was amplified by primers ire-h1CDS(A)5P-*Bam*HI and ire-h1CDS(B)3P-*Sac*I, and cloned into *pGADT7* with *Bam*HI and *Sac*I to generate *pGADT7-IREH1*. The full-length CDS (without the stop codon) of *IRE3* was amplified by primers IRE3-5P-*Nco*I and IRE3-3P-*Sal*I(nsc), and cloned into *pGBKT7* with *Nco*I and *Sal*I to generate *pGBKT7-IRE3*. The full-length CDS (without the stop codon) of *IRE3* was amplified by primers IRE3-5P-*Xma*I and IRE3-3P-*Xho*I(nsc), and cloned into *pGADT7* with *Xma*I and *Xho*I to generate *pGADT7-IRE3*.

For the Co-IP assay, the full-length CDS (without the stop codon) of *IREH1* was amplified by primers ireh1CDS-5P-*Xba*I and ireh1CDS-3P-linker-*Apa*I(nsc), and cloned into *pSuper1300-Flag*

with *Xba*I and *Apa*I to generate *pSuper1300-IREH1-Flag*. The full-length CDS (without the stop codon) of *IRE3* was amplified by primers IRE3-5P-*Apa*I and IRE3-3P-*Sal*I(nsc), and cloned into *pSuper1300-GFP* with *Apa*I and *Sal*I to generate *pSuper1300-IRE3-GFP*.

For the LCI assay, the full-length CDS (without the stop codon) of *IREH1* was amplified by primers IREH1-nLUC-F and IREH1-nLUC-R(nsc), and cloned into *pCAMBIA1300-nLUC* to generate *pCAMBIA1300-IREH1-nLUC* by using Gibson assembly method. Similarly, the full-length CDS of *IRE3* was amplified by primers IRE3-cLUC-F and IRE3-cLUC-R, and cloned into *pCAMBIA1300-cLUC* to produce *pCAMBIA1300-cLUC-IRE3*.

The primers used for generating the constructs are listed in Table S3.

4.5. GUS staining

GUS assays were carried out as previously described (Cheng et al., 2006; Cui et al., 2016). To analyze the expression patterns of *IREH1* and *IRE3*, the transgenic plants harboring *pPZP211-IREH1gDNA-GUS* or *pPZP211-IRE3gDNA-GUS* were observed after GUS staining.

4.6. Microscopy and image analysis

GUS staining samples and root epidermal cells were photographed using differential interference contrast (DIC) field on DM 4500 and S8AP0 microscopes (Leica, Germany). The *KNpro*:EGFP-MBD signals were observed and captured with FV1000MPE confocal microscope (Olympus, Japan) following the manufacturer's instructions.

For the measurements of fluorescence intensity and arrangement of *KNpro*:EGFP-MBD labeled microtubules, images were scanned on confocal microscope with same settings for each root zone. The fluorescence intensities of merged images (1 μm thickness in meristem zone, and 2.5 μm thickness in elongation zone and maturation zone) were measured using ImageJ. The value of WT was set as an arbitrary unit 1. The fluorescence signals of 45 epidermal cells per genotype (15 roots and 3 epidermal cells per root) were measured. To quantify the microtubule arrangement in the maturation zone, 75 cells per genotype (25 roots and 3 epidermal cells per root) were measured. The angles were determined by the left side of the cell and the microtubule arrays (Fig. 3G).

4.7. IP-MS assay

To identify the IREH1-interacting proteins, *pPZP211-IREH1gDNA-GFP* was transformed into *ireh1-1* to generate transgenic plants. The T_2 plants with the *IREH1-GFP* transgene were used as the sample and the plants with the *GFP* transgene as a control. Total proteins were extracted from 1 g of aerial parts of 6-week-old plants with 2.5 mL extraction buffer (50 mM HEPES pH 7.5, 100 mM NaCl, 0.5% (v/v) Triton X-100, 1 mM DTT, 10 μL to 1 mL protease inhibitor cocktail (Sigma, USA), 1× PhosSTOP (Roche, Germany), 50 μM MG132). The protein extracts were kept on ice for 30 min and spun for 30 min at 18,000 *g* at 4 °C. The supernatant was filtered using calbiochem miracloth (Millipore, USA) and incubated with anti-GFPmAb-agarose (MBL, USA) for 1 h at 4 °C with gentle shaking. The agarose was washed three times with washing buffer (50 mM HEPES pH 7.5, 100 mM NaCl, 0.5% (v/v) Triton X-100, 1 mM DTT). Proteins were eluted into 40 μL 2× SDS loading buffer by boiling for 5 min. After separated on SDS-PAGE gel and Coomassie blue staining, the gel stripes with proteins were cut and in-gel digestion was performed. Acetonitrile:50 mM ammonium bicarbonate (1:1, v/v) was added to de-stain the excised gel spots. The gel particles were dried twice using acetonitrile, and kept in 10 mM DTT solution at 56 °C for 1 h. Subsequently, the same volume of 50 mM iodoacetamide was added and incubated at room temperature in dark for 1 h. The solution was removed and the gel particles were dried twice using acetonitrile. The trypsin solution (0.01 μg/μL containing 25 mM ammonium bicarbonate; Promega, USA) was added to the gel particles, and incubated at 4 °C for 1 h then at 37 °C for 16–18 h. The candidate IREH1-interacting proteins were identified by Mass Spectrometry (1D/2D ultra plus/5600+; AB SCIEX, USA).

4.8. Yeast two-hybrid assay

For the yeast two-hybrid assay, the CDSs of *IREH1* and *IRE3* were cloned into *pGBKT7* and *pGADT7*, respectively. The interaction of IREH1 and IRE3 was tested according the manufacturer's user manual (Matchmaker® Gold Yeast Two-Hybrid System, Clontech, USA) in AH109.

4.9. Co-IP assay

For the Co-IP assay of IREH1 and IRE3, *pSuper1300-IREH1-Flag* and *pSuper1300-IRE3-GFP* were first transformed into *Agrobacterium tumefaciens* strain GV3101, respectively. The two suspensions of *Agrobacterium* were mixed equally and injected into *N. benthamiana* leaves. Three days after injection, the leaves were collected and homogenized in liquid nitrogen, re-suspended with protein extraction buffer (1:1, v/v) (100 mM HEPES pH 7.5, 5 mM EDTA, 5 mM EGTA, 10 mM NaF, 5% Glycerol, 10 mM Na_3VO_4, 10 mM DTT, 1 mM PMSF, 10 μL to 1 mL protease inhibitor cocktail (Sigma), 0.5% Triton X-100). The supernatant and 5× IP buffer (100 mM Tris-HCl pH 7.5, 750 mM NaCl, 5 mM EDTA, 5 mM EGTA, 5 mM Na_3VO_4, 5 mM NaF, 50 mM β-glycerophosphate, 0.5% Triton X-100) were mixed and incubated with anti-GFPmAb-agarose (MBL) for 1 h at 4 °C. The agarose was washed three times using PBS and boiled for 5 min in 2× SDS loading buffer. The eluted proteins were examined by immunoblotting using anti-Flag and anti-GFP antibodies.

4.10. LCI assay

For the LCI assay of IREH1 and IRE3, *pCAMBIA1300-IREH1-nLUC* and *pCAMBIA1300-cLUC-IRE3* were first transformed into *Agrobacterium tumefaciens* strain GV3101, respectively. The two suspensions of *Agrobacterium* were mixed equally and injected into *N. benthamiana* leaves. Leaves were collected 3 days after injection and incubated in the D-luciferin solution (Goldbio, USA) for 3 min in dark. The luciferase signals were analyzed by Chemiluminescent Imaging System (Tanon 5200, China). The exposure time was 5–10 min.

4.11. Statistical analysis

Data are presented as mean ± SE. Statistical analysis was performed using a one-way ANOVA followed by LSD test.

Acknowledgments

We thank Drs. Yongbiao Xue, Zhaosheng Kong, Jie Le for discussion, Dr. Shanjin Huang for the microtubule marker *KNpro*:EGFP-MBD, Dr. Yuxin Hu for the Chemiluminescent Imaging System, Dr. Jianmin Zhou for the LCI system vectors, Drs. Zhaosheng Kong, Jingquan Li and Chaofeng Wang for help on observing microtubule marker. This work was supported by the grants from the National Natural Science Foundation of China (31270330, 91217310, 91017008 and 31171389), the National Basic Research Program of China (2014CB943400), the National Key Research and

Development Program of China (2016YFD0100402), the Strategic Priority Research Program of the Chinese Academy of Sciences (XDA0801010402), and the One-Hundred Talent Project of the Chinese Academy of Sciences to Y.C.

Supplementary data

Supplementary data to this article can be found online at https://doi.org/10.1016/j.jgg.2019.02.007.

References

Barbosa, I.C.R., Hammes, U.Z., Schwechheimer, C., 2018. Activation and polarity control of PIN-FORMED auxin transporters by phosphorylation. Trends Plant Sci. 23, 523–538.

Baskin, T.I., Wilson, J.E., Cork, A., Williamson, R.E., 1994. Morphology and microtubule organization in *Arabidopsis* roots exposed to oryzalin or taxol. Plant Cell Physiol. 35, 935–942.

Bisgrove, S.R., Lee, Y.R., Liu, B., Peters, N.T., Kropf, D.L., 2008. The microtubule plus-end binding protein EB1 functions in root responses to touch and gravity signals in *Arabidopsis*. Plant Cell 20, 396–410.

Bögre, L., 2003. Growth signalling pathways in *Arabidopsis* and the AGC protein kinases. Trends Plant Sci. 8, 424–431.

Briggs, W.R., Christie, J.M., 2002. Phototropins 1 and 2: versatile plant blue-light receptors. Trends Plant Sci. 7, 204–210.

Cheng, Y., Dai, X., Zhao, Y., 2006. Auxin biosynthesis by the YUCCA flavin monooxygenases controls the formation of floral organs and vascular tissues in *Arabidopsis*. Genes Dev. 20, 1790–1799.

Cheng, Y., Qin, G., Dai, X., Zhao, Y., 2008. *NPY* genes and AGC kinases define two key steps in auxin-mediated organogenesis in *Arabidopsis*. Proc. Natl. Acad. Sci. U. S. A. 105, 21017–21022.

Chudinova, E.M., Karpov, P.A., Fokin, A.I., Yemets, A.I., Lytvyn, D.I., Nadezhdina, E.S., Blume, Y.B., 2017. MAST-like protein kinase IREH1 from *Arabidopsis thaliana* co-localizes with the centrosome when expressed in animal cells. Planta 246, 959–969.

Christensen, S.K., Dagenais, N., Chory, J., Weigel, D., 2000. Regulation of auxin response by the protein kinase PINOID. Cell 100, 469–478.

Clough, S.J., Bent, A.F., 1998. Floral dip: a simplified method for *Agrobacterium*-mediated transformation of *Arabidopsis thaliana*. Plant J. 16, 735–743.

Cui, X., Guo, Z., Song, L., Wang, Y., Cheng, Y., 2016. NCP1/AtMOB1A plays key roles in auxin-mediated *Arabidopsis* development. PLoS Genet. 12, e1005923.

de la Fuente van Bentem, S., Anrather, D., Dohnal, I., Roitinger, E., Csaszar, E., Joore, J., Buijnink, J., Carreri, A., Forzani, C., Lorkovic, Z.J., Barta, A., Lecourieux, D., Verhounig, A., Jonak, C., Hirt, H., 2008. Site-specific phosphorylation profiling of *Arabidopsis* proteins by mass spectrometry and peptide chip analysis. J. Proteome Res. 7, 2458–2470.

Enugutti, B., Kirchhelle, C., Oelschner, M., Torres Ruiz, R.A., Schliebner, I., Leister, D., Schneitz, K., 2012. Regulation of planar growth by the *Arabidopsis* AGC protein kinase UNICORN. Proc. Natl. Acad. Sci. U. S. A. 109, 15060–15065.

Furutani, I., Watanabe, Y., Prieto, R., Masukawa, M., Suzuki, K., Naoi, K., Thitamadee, S., Shikanai, T., Hashimoto, T., 2000. The *SPIRAL* genes are required for directional control of cell elongation in *Arabidopsis thaliana*. Development 127, 4443–4453.

Gibson, D.G., Young, L., Chuang, R.Y., Venter, J.C., Hutchison III, C.A., Smith, H.O., 2009. Enzymatic assembly of DNA molecules up to several hundred kilobases. Nat. Methods 6, 343–345.

Haga, K., Frank, L., Kimura, T., Schwechheimer, C., Sakai, T., 2018. Roles of AGCVIII kinases in the hypocotyl phototropism of *Arabidopsis* seedlings. Plant Cell Physiol. 59, 1060–1071.

Hain, D., Langlands, A., Sonnenberg, H.C., Bailey, C., Bullock, S.L., Muller, H.A., 2014. The *Drosophila* MAST kinase Drop out is required to initiate membrane compartmentalisation during cellularisation and regulates dynein-based transport. Development 141, 2119–2130.

Hasenstein, K.H., Blancaflor, E.B., Lee, J.S., 1999. The microtubule cytoskeleton does not integrate auxin transport and gravitropism in maize roots. Plant Physiol. 105, 729–738.

Hajdukiewicz, P., Svab, Z., Maliga, P., 1994. The small, versatile *pPZP* family of *Agrobacterium* binary vectors for plant transformation. Plant Mol. Biol. 25, 989–994.

Karpov, P.A., Nadezhdina, E.S., Yemets, A.I., Matusov, V.G., Nyporko, A.Y., Shashina, N.Y., Blume, Y.B., 2010. Bioinformatic search of plant microtubule- and cell cycle related serine-threonine protein kinases. BMC Genomics 11 (Suppl. 1), S14.

Marhava, P., Bassukas, A.E.L., Zourelidou, M., Kolb, M., Moret, B., Fastner, A., Schulze, W.X., Cattaneo, P., Hammes, U.Z., Schwechheimer, C., Hardtke, C.S., 2018. A molecular rheostat adjusts auxin flux to promote root protophloem differentiation. Nature 558, 297–300.

Morejohn, L.C., 1991. The molecular pharmacology of plant tubulin and microtubules. In: Lloyd, C. (Ed.), The Cytoskeletal Basis of Plant Growth and Form. Academic Press, London, pp. 29–43.

Naoi, K., Hashimoto, T., 2004. A semidominant mutation in an *Arabidopsis* mitogen-activated protein kinase phosphatase-like gene compromises cortical microtubule organization. Plant Cell 16, 1841–1853.

Nemoto, K., Seto, T., Takahashi, H., Nozawa, A., Seki, M., Shinozaki, K., Endo, Y., Sawasaki, T., 2011. Autophosphorylation profiling of *Arabidopsis* protein kinases using the cell-free system. Phytochemistry 72, 1136–1144.

Nakajima, K., Furutani, I., Tachimoto, H., Matsubara, H., Hashimoto, T., 2004. *SPIRAL1* encodes a plant-specific microtubule-localized protein required for directional control of rapidly expanding *Arabidopsis* cells. Plant Cell 16, 1178–1190.

Oyama, T., Shimura, Y., Okada, K., 2002. The *IRE* gene encodes a protein kinase homologue and modulates root hair growth in *Arabidopsis*. Plant J. 30, 289–299.

Pearce, L.R., Komander, D., Alessi, D.R., 2010. The nuts and bolts of AGC protein kinases. Nat. Rev. Mol. Cell Biol. 11, 9–22.

Perrin, R.M., Wang, Y., Yuen, C.Y.L., Will, J., Masson, P.H., 2007. WVD2 is a novel microtubule-associated protein in *Arabidfopsis thaliana*. Plant J. 49, 961–971.

Qi, B., Zheng, H., 2013. Modulation of root-skewing responses by *KNAT1* in *Arabidopsis thaliana*. Plant J. 76, 380–392.

Roy, R., Bassham, D.C., 2014. Root growth movements: waving and skewing. Plant Sci. 221–222, 42–47.

Roy, R., Bassham, D.C., 2017. TNO1, a TGN-localized SNARE-interacting protein, modulates root skewing in *Arabidopsis thaliana*. BMC Plant Biol. 17, 73.

Sedbrook, J., Ehrhardt, D., Fisher, S., Scheible, W., Somerville, C., 2004. The *Arabidopsis SKU6/SPIRAL1* gene encodes a plus end-localized microtubule-interacting protein involved in directional cell expansion. Plant Cell 16, 1506–1520.

Shoji, T., Narita, N.N., Hayashi, K., Asada, J., Hamada, T., Sonobe, S., Nakajima, K., Hashimoto, Y., 2004. Plant-specific microtubule-associated protein SPIRAL2 is required for anisotropic growth in *Arabidopsis*. Plant Physiol. 136, 3933–3944.

Thitamadee, S., Tuchihara, K., Hashimoto, T., 2002. Microtubule basis for left-handed helical growth in *Arabidopsis*. Nature 417, 193–196.

Valiente, M., Andres-Pons, A., Gomar, B., Torres, J., Gil, A., Tapparel, C., Antonarakis, S.E., Pulido, R., 2005. Binding of PTEN to specific PDZ domains contributes to PTEN protein stability and phosphorylation by microtubule-associated serine/threonine kinases. J. Biol. Chem. 280, 28936–28943.

Vaughn, L.M., Masson, P.H., 2011. A QTL study for regions contributing to *Arabidopsis thaliana* root skewing on tilted surfaces. G3 1, 105–115.

Wang, Q., Huang, S., 2014. Visualization of microtubule organization and dynamics in living *Arabidopsis* embryonic cells. Mol. Plant 7, 1397–1401.

Willige, B.C., Ahlers, S., Zourelidou, M., Barbosa, I.C., Demarsy, E., Trevisan, M., Davis, P.A., Roelfsema, M.R., Hangarter, R., Fankhauser, C., Schwechheimer, C., 2013. D6PK AGCVIII kinases are required for auxin transport and phototropic hypocotyl bending in *Arabidopsis*. Plant Cell 25, 1674–1688.

Whittington, A.T., Vugrek, O., Wei, K.J., Hasenbein, N.G., Sugimoto, K., Rashbrooke, M.C., Wasteneys, G.O., 2001. MOR1 is essential for organizing cortical microtubules in plants. Nature 411, 610–613.

Zourelidou, M., Muller, I., Willige, B.C., Nill, C., Jikumaru, Y., Li, H., Schwechheimer, C., 2009. The polarly localized D6 PROTEIN KINASE is required for efficient auxin transport in *Arabidopsis thaliana*. Development 136, 627–636.